# Micro-CT analysis of the internal deformed geometry of a non-crimp 3D orthogonal weave E-glass composite reinforcement

Juan Pazmino [a], Valter Carvelli [a,*], Stepan V. Lomov [b]

[a] Department of Architecture, Built Environment and Construction Engineering, Politecnico di Milano, Piazza Leonardo da Vinci 32, 20133 Milan, Italy
[b] Department of Metallurgy and Materials Engineering, KU Leuven, Kasteelpark Arenberg 44, B-3001 Leuven, Belgium

Received 5 June 2013
Received in revised form 4 October 2013 Accepted 20 November 2013
Available online 28 November 2013

## 1. Introduction

During forming and molding processes of composite reinforcements it is generally agreed that the most relevant deformation mechanisms occurring are in-plane shear, biaxial tensile and through-thickness compaction [1]. Of these mechanisms, the ability of fabrics to shear in-plane is the most important feature during forming of textile reinforcements to complex (three-dimensional) shapes [1,2].

Deformation mechanisms occurring during draping processes of composite reinforcements can be classified according to the length scale over which they occur. Indeed, deformations at the scale of a composite component (macroscopic scale) correspond to local deformations of the fibrous network (mesoscopic scale), which can modify the mechanical properties and the permeability of the reinforcement [3]. The knowledge of the interlacement modifications during shaping deformation is of fundamental importance in predicting the features of a composite material reinforced with textile. Several researches have been dedicated to measure the internal geometry mainly of two-dimensional textile reinforcements (see e.g. [3,4]). Few works considered three-dimensional reinforcements [5,6]. Those experimental data allow having realistic solid model for numerical modeling and accurate prediction of the mechanical behavior of textile reinforcements [7], including the transverse compaction effect [8] arising during composite forming and manufacturing.

In this work, an investigation at the unit cell level of the sheared geometry of a single layer E-glass non-crimp 3D orthogonal woven reinforcement (commercialized under trademark 3WEAVE® by 3Tex Inc.) is performed by X-ray micro-computed tomography (micro-CT) observations. The aim of this study is to observe, understand and quantify the effect of in-plane shear deformation (applied in a picture frame test), on the composite reinforcement geometry at the mesoscopic scale (i.e. unit cell level). The information gathered from micro-CT analyses has an important role in the generation of an accurate virtual model for numerical simulations with such 3D composite reinforcement.

Furthermore, in the composite component production process, after the forming of the reinforcement into a desired shape, a vacuum is applied which compresses it transversely. The thickness and the related fiber volume fractions are consequences of the applied compression and of the deformation imposed to the reinforcement during shaping which depends mainly on the in-plane shear [1,2]. The coupled effect of shear deformation and transversal pressure, as in forming and molding phases, is investigated recording the textile thickness during compression test of sheared specimens.

* Corresponding author. Tel.: +39 02 23994354.
*E-mail address:* valter.carvelli@polimi.it (V. Carvelli).

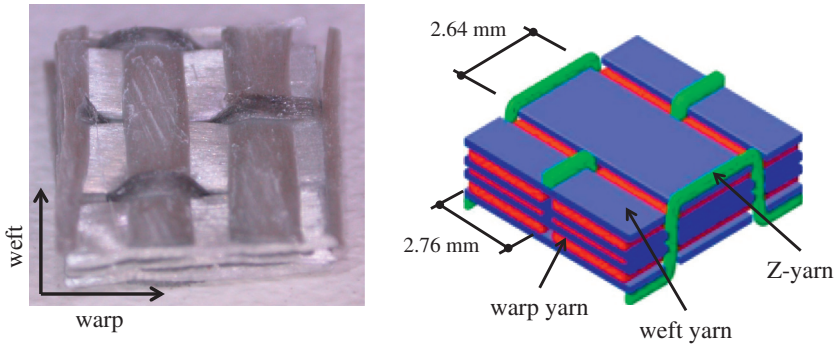


**Fig. 1.** Architecture of the tows inside the non-crimp 3D orthogonal weave preform [8].

**Table 1**
Properties of the non-crimp 3D orthogonal weave preform. Data provided by 3Tex Inc.

| | | |
|---|---|---|
| | Fabric plies | 1 |
| | Areal density (g/m) | 3255 |
| Warp | Insertion density (ends/cm) | 2.76 |
| | Top and bottom layer yarns (tex) | 2275 |
| | Middle layer yarns (tex) | 1100 |
| Weft | Insertion density (ends/cm) | 2.64 |
| | Yarns (tex) | 1470 |
| Z-yarns | Insertion density (ends/cm) | 2.76 |
| | Yarns (tex) | 1800 |

## 2. Material characteristics

The fabric is a single layer E-glass non-crimp 3D orthogonal woven reinforcement (commercialized under trademark 3WEAVE® by 3Tex Inc.). The fiber architecture of the preform has three warp and four weft layers, interlaced by through thickness (*Z*-directional) yarns (see Fig. 1 [9]). The fabric construction results in ~49%/~49%/~2% ratio of the fiber amounts (by volume) in the warp, weft and Z fiber directions, respectively. The same 3D fabric was experimentally investigated as dry reinforcement in [5,10] and as composite material in [9,11]. The textile preform is produced by means 3D orthogonal weaving technology in 3Tex Inc. [12]. A detailed description of the 3D orthogonal weaving production process is presented in [13]. The fibre material is PPG Hybon 2022 E-glass. Some features of the non-crimp 3D orthogonal weave reinforcement are listed in Table 1. The reader is referred to [5] for detailed description of the preform architecture, studied with optical microscopy and micro-CT.

## 3. Experimental techniques and methodologies

In order to gather information about the internal geometry variation due to in-plane shear deformation of the non-crimp 3D orthogonal woven fabric, X-ray micro-computed tomography (micro-CT) analyses were carried out on a reference sample at the unloaded state, and on specimens which have undergone shear deformation for shear angle of 15°, 20°, 25° and 30° after picture frame tests. Moreover, fabric thickness measurements from micro-CT observations were compared with those obtained by compression tests on sheared specimens.

### 3.1. Picture frame test

The picture frame shear test consists in clamping a fabric on a hinged frame whose sides directions are those of the fabric yarns [14]. Different configurations of the setup exist in laboratories all over the world (see e.g. [15]). In the present study the setup available in K.U.Leuven (see Fig. 2a) was used.

The frame was mounted on an Instron 5567 tensile machine. A test speed of 10 mm/min and a maximum displacement of 12 mm, corresponding to a frame shear angle of 30°, were set. The tested samples had the cross-like shape depicted in Fig. 2b. The adopted procedure and more details of the picture frame test for the considered 3D reinforcement are mentioned in [10].

Three load–unload cycles have been performed to allow the accommodation of the fabric in the frame clamping. The load vs. shear angle diagram shows very similar second and third cycle (see [10]). Therefore, it was decided to consider the reinforcement in the second cycle to prepare specimens for micro-CT

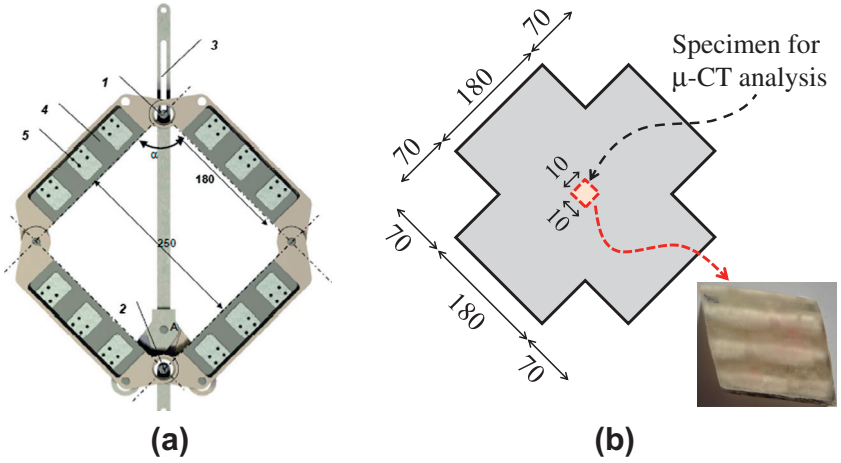


**Fig. 2.** (a) Picture frame sketch; (b) picture frame and μ-CT specimen (dimensions in mm).

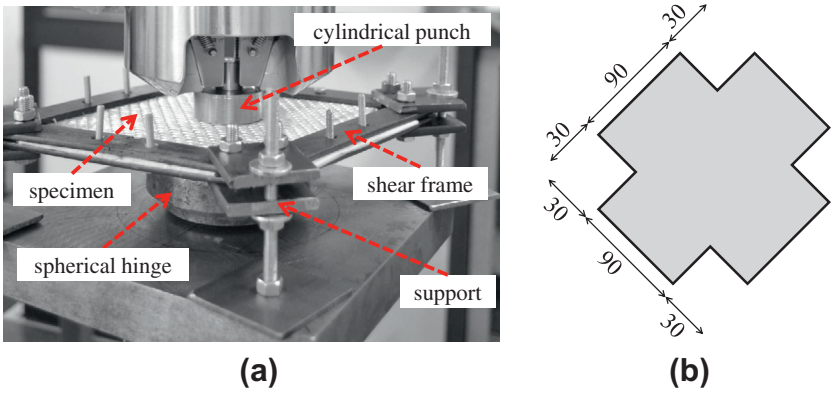


**Fig. 3.** Shear and compression test: (a) set-up; (b) specimen geometry (dimensions in mm).

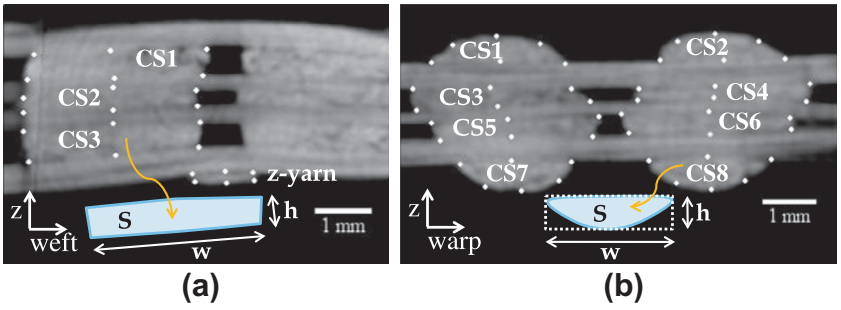


**Fig. 4.** (a) 'Z-weft' cross-section; and (b) 'Z-warp' cross-section of the non-crimp 3D orthogonal woven reinforcement unit cell. Identification of the yarns transversal cross-sections: (a) warp yarns cross-sections and (b) weft yarns cross-sections.

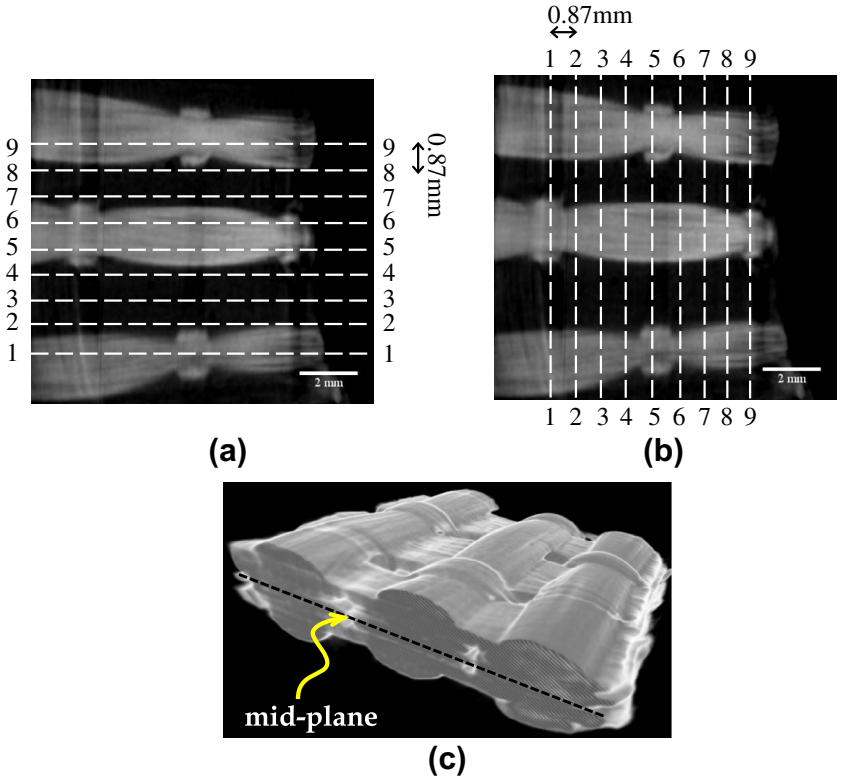


**Fig. 5.** Position of (a) 'Z-weft' cross-sections and (b) 'Z-warp' cross-sections. (c) Three-dimensional view of an observed cell.

**Table 2**
Yarns cross-section geometric features of the unsheared reinforcement.

| | Cross-section | 1-1 | 2-2 | 3-3 | 4-4 | 5-5 | 6-6 | 7-7 | 8-8 | 9-9 |
|---|---|---|---|---|---|---|---|---|---|---|
| $S_0$ $(mm^2)$ | | | | | | | | | | |
| Warp | CS1–CS3 | 1.05 | 1.15 | 1.11 | 1.15 | 1.19 | 1.14 | 1.37 | 1.21 | 1.33 |
| Yarns | CS2 | 0.57 | 0.58 | 0.50 | 0.68 | 0.78 | 0.68 | 0.75 | 0.79 | 0.73 |
| Weft | CS1-2-7-8 | 0.85 | 0.86 | 0.83 | 0.81 | 0.76 | 0.78 | 0.74 | 0.75 | 0.74 |
| Yarns | CS3-4-5-6 | 0.95 | 1.11 | 1.02 | 0.96 | 0.75 | 0.94 | 0.86 | 0.86 | 0.72 |
| $w_0$ $(mm)$ | | | | | | | | | | |
| Warp | CS1-CS3 | 2.82 | 2.83 | 2.77 | 2.68 | 2.78 | 2.84 | 3.10 | 2.84 | 2.92 |
| Yams | CS2 | 2.86 | 2.77 | 2.77 | 2.79 | 2.93 | 2.73 | 3.07 | 2.77 | 2.89 |
| Weft | CS1-2-7-8 | 2.31 | 2.32 | 2.30 | 2.27 | 2.19 | 2.22 | 2.18 | 2.16 | 2.08 |
| Yams | CS3-4-5-6 | 3.33 | 3.35 | 3.22 | 3.16 | 3.11 | 3.07 | 2.99 | 2.99 | 2.95 |
| $h_0$ $(mm)$ | | | | | | | | | | |
| Warp | CS1-CS3 | 0.50 | 0.50 | 0.48 | 0.49 | 0.52 | 0.54 | 0.56 | 0.52 | 0.60 |
| Yams | CS2 | 0.25 | 0.23 | 0.25 | 0.28 | 0.34 | 0.30 | 0.37 | 0.37 | 0.30 |
| Weft | CS1-2-7-8 | 0.57 | 0.58 | 0.56 | 0.54 | 0.53 | 0.54 | 0.52 | 0.54 | 0.58 |
| Yams | CS3-4-5-6 | 0.40 | 0.43 | 0.40 | 0.38 | 0.33 | 0.39 | 0.38 | 0.38 | 0.40 |

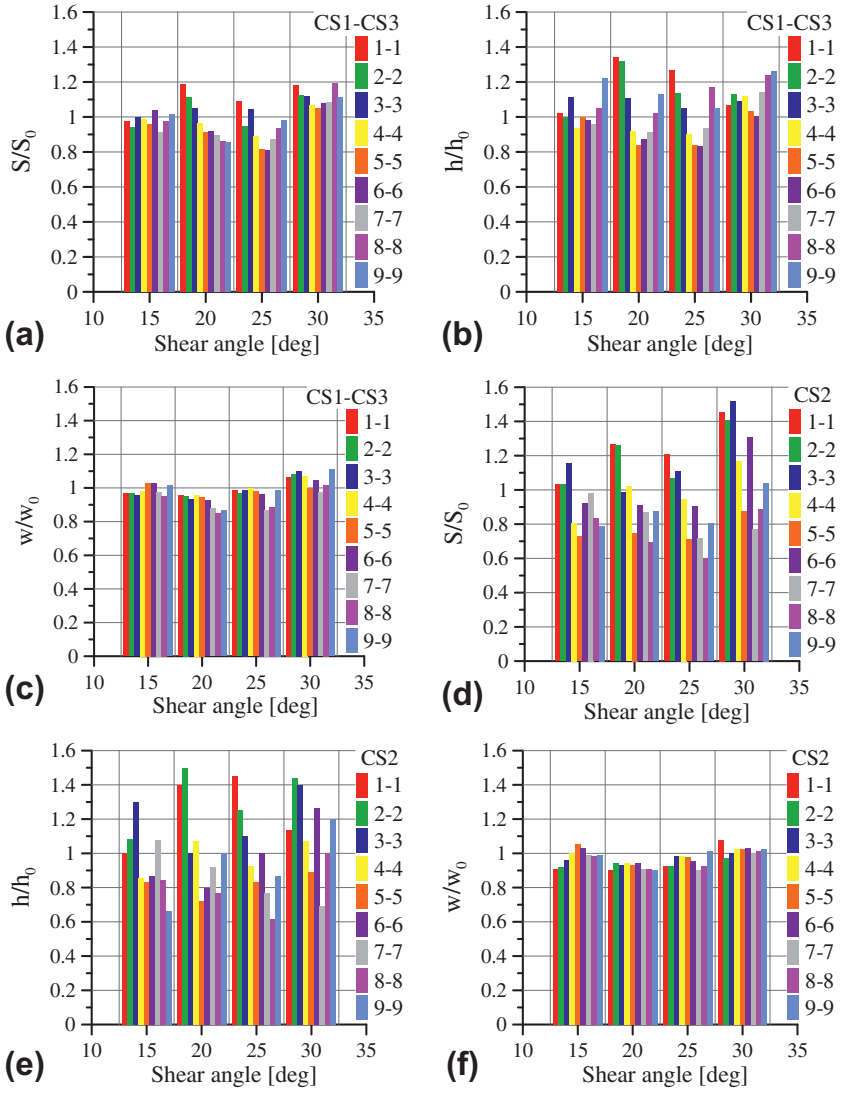


**Fig. 6.** Warp yarns shape parameters vs. shear angle, for the nine positions analyzed. Average measurements of cross-sections CS1 and CS3: (a) $S/S_0$; (b) $h/h_0$; (c) $w/w_0$. Measurements of cross-section CS2: (d) $S/S_0$; (e) $h/h_0$; (f) $w/w_0$.

observations. Picture frame tests were interrupted, during the second loading cycle at shear angles of 15°, 20°, 25° and 30°. For each angle, the deformed configuration in the central part of the sample ($150 \times 150$ mm) was fixed using a single-component cyanoacrylate adhesive. Afterwards, the sample was rigidified by a coating of epoxy resin applied mainly on the external surfaces. Finally, a

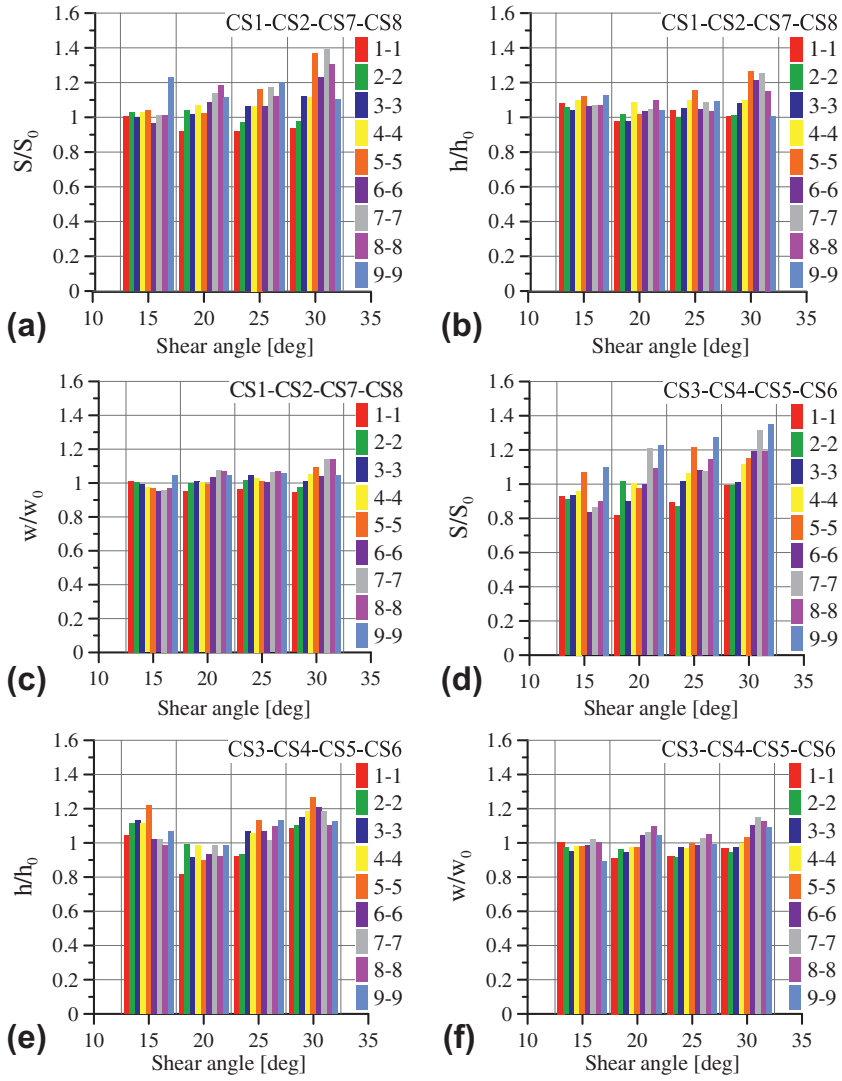


**Fig. 7.** Weft yarns shape parameters vs. shear angle, for the nine positions analyzed. Average measurements of cross-sections CS1, CS2, CS7, CS8: (a) $S/S_0$; (b) $h/h_0$; (c) $w/w_0$. Average measurements of cross-section CS3, CS4, CS5, CS6: (d) $S/S_0$; (e) $h/h_0$; (f) $w/w_0$.

specimen (one for each shear angle) correspondent to the non-crimp 3D orthogonal woven reinforcement unit cell (≈10 × 10 mm), was extracted from the center (see Fig. 2b), using a diamond saw. This specimen preparation procedure, is similar to the one adopted for microscopy investigations in [16].

### 3.2. X-ray micro-computed tomography (micro-CT) setup

Microfocus X-ray Computed Tomography (micro-CT) is a non-destructive technique which allows three-dimensional observation of the internal structure of a material. The principles of the technique are detailed in [17,18]. In the field of fibre reinforced polymer composites, X-ray micro-CT has been used mainly for two types of investigations: to study damage mechanisms (e.g. [19,20]); and to observe the internal geometry of composite reinforcements in relaxed state (e.g. [5,21]) and after biaxial and/or shear deformation (see e.g. [3,22]). Concerning the study of fabrics internal geometry, the information gathered from micro-CT is used to improve the solid models adopted in finite element simulations of the mechanical behavior of the reinforcements or of the related composite materials [7].

In the present work, a Philips HOMX 161 X-ray system (Philips X-ray, Germany) with the AEA Tomohawk upgrade (AEA Technology, UK) was used for micro-CT images acquisition. Its detector system has an image intensifier TH 9428HX and a CCD camera (1024 × 1024 pixels) 12 bit dynamic range. The scans were performed by X-rays at a tube voltage of 80 kV, current of 0.5 mA and using an aluminium filter 1 mm thick. During the acquisition, the specimen was rotated over 187.8° in steps of 0.3°. After each rotation, 32 images were acquired and the average radiograph was saved, resulting in a total of 626 radiographic images. These were assembled into cross-sectional images with a commercial software package NRecon (Skyscan N.V., Kontich, Belgium). The reconstructed micro-CT dataset had an isotropic voxel size of 22.9 $\mu m^3$. This dataset was further analyzed using the open source software ImageJ [23], and the commercially available image analysis software Data Viewer (Skyscan N.V., Kontich, Belgium) [24,25].

### 3.3. Shear and transverse compression test

During the compaction stage of resin infusion processes, one of the main deformation mode introduced during draping is the in-plane shear, combined with transversal compression [8], due to the applied vacuum and possible additional weights, which modifies the final material thickness. The response of the reinforcement in term of thickness variation is an important knowledge for the

prediction of the fiber content in the composite component and, as consequence, of the mechanical properties.

The thickness of the considered 3D fabric during shear and transversal compression was experimentally measured with a set-up similar to the one detailed in [26]. It consists of a metallic cylindrical punch of diameter 40 mm applying compressive pressure, and a metal frame which allows fabric in-plane shear deformation up to an angle of 30°. A spherical hinge was adopted to uniformly distribute the pressure on the contact surface. The shear-compression test set-up is illustrated in Fig. 3a; while the samples geometry is depicted in Fig. 3b.

First a calibration curve is recorded to account for the machine compliance. After calibration, fabric specimens are inserted and clamped in the shear frame in the initial position (0° shear). The frame is then sheared up to the desired shear angle and locked. The sheared frame is positioned on four holders with adjustable height to have the initial contact between the fabric and the spherical hinge (see Fig. 3a). The spherical hinge allows a uniform punch pressure reducing the possible slight error of parallelism between the punch and textile plane.

Three load–unload cycles have been performed assuming an initial pre-load of 5 N. The thickness vs. pressure diagram has been deduced subtracting the calibration curve from the load–displacement data of each specimen and assuming a constant compressed circular surface of 40 mm diameter.

A MTS 858 Bionix machine, with a load cell of 2.5 kN has been used. The maximum applied pressure in each cycle was 2 MPa. Three tests for each shear angle (0°, 15°, 20°, 25°, 30°) have been performed.

## 4. Results

### 4.1. Micro-CT analyses

X-ray micro-computed tomography cross-sectional images of sheared specimens, corresponding to a unit cell of to the non-crimp 3D orthogonal woven reinforcement, were analyzed following the procedures adopted in [5,6].

In the following, a cross section is named 'Z-weft', if it contains the longitudinal cross sections of the weft yarns and transverse cross sections of the warp yarns (see Fig. 4a). While, a cross section is called 'Z-warp' when it shows the longitudinal cross sections of the warp yarns and transverse cross sections of the weft yarns (see Fig. 4b).

One sample has been investigated for each shear angle (i.e. 0°, 15°, 20°, 25° and 30°) and nine 'Z-warp' and 'Z-weft' images, correspondent to 18 different positions in the fabric unit cell (see Fig. 5), were processed. Hence, a total of 90 cross-sectional images were analyzed. Each cross-section is obtained with a plane orthogonal to the reinforcement mid-plane (Fig. 5c). In the undeformed state, the distance between two adjacent cross-sections was established to 38 pixel, corresponding to 0.87 mm (see Fig. 5). For sheared specimens, due to deformation mechanisms, the distance of the cross-sections have been maintained as close as possible to the ones in the undeformed state.

The micro-computed tomography pictures allowed measuring the yarns cross-section features, the yarns crimp and the yarns spacing in the sheared deformed configuration considered.

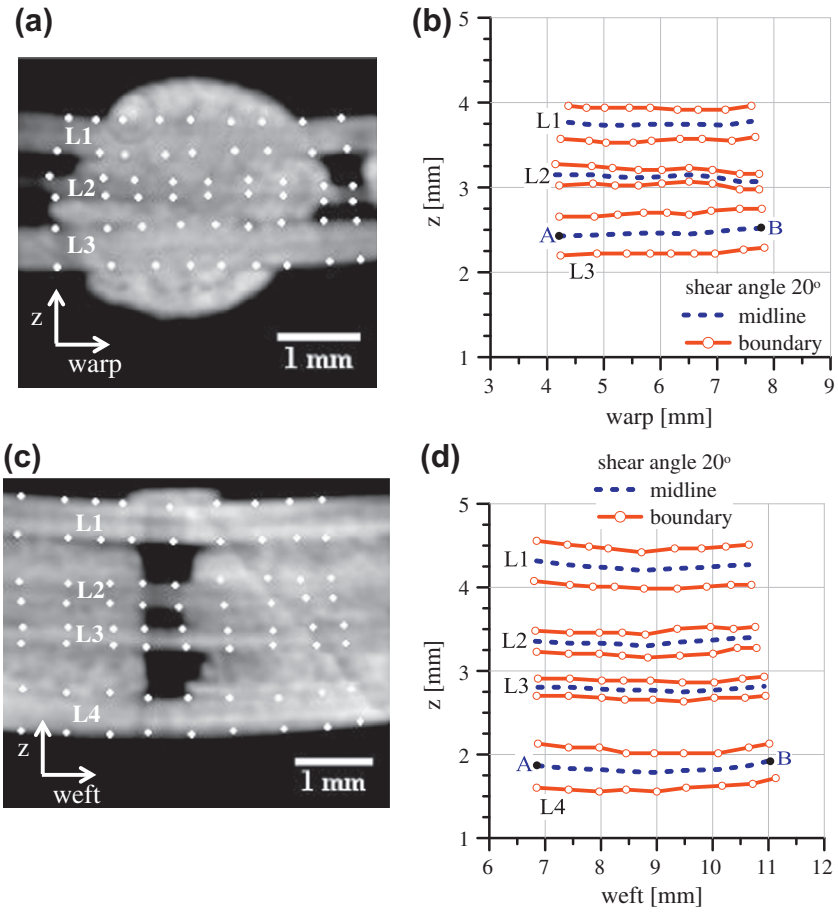


**Fig. 8.** Measurement of the yarns longitudinal cross-sections of a specimen sheared up to 20°. Scheme of measurement for (a) Z-warp cross-section 2-2 and (c) Z-weft cross-section 1-1, and boundaries and mid-lines of (b) warp and (d) weft yarns.

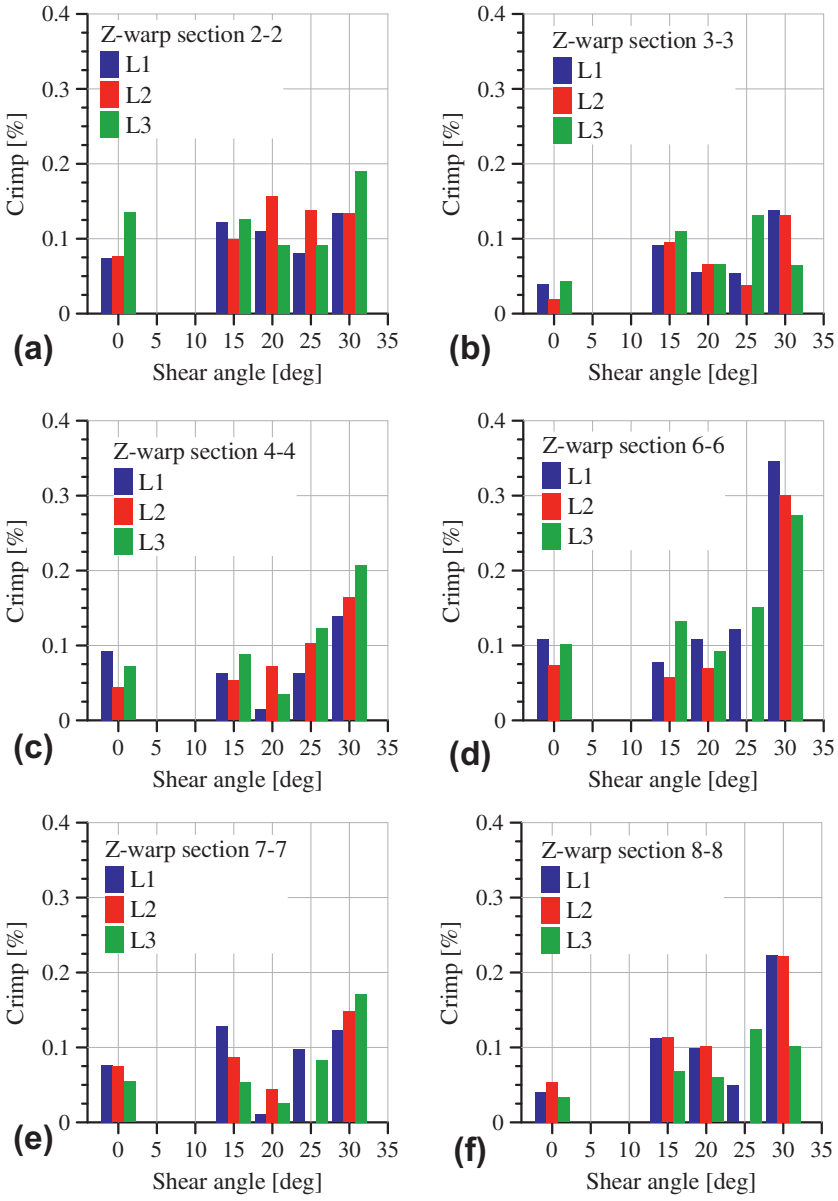


**Fig. 9.** Warp yarns crimp variation vs. shear angle, for positions: (a) 2-2; (b) 3-3; (c) 4-4; (d) 6-6; (e) 7-7; and (f) 8-8 in Fig. 5b.

*4.1.1. Warp and weft yarns cross-sections*

Yarns transversal cross-sections in plane 'Z-warp' and 'Z-weft' are named as in Fig. 4. For each position (see Fig. 5), three warp (Fig. 4a) and eight weft (see Fig. 4b) yarns were measured. Only three warp yarns cross-sections were considered in the analyses whose measurements are considered reliable (Fig. 4a). It is important to notice that, unlike in situ measurements, as performed in [22], the sample preparation process for micro tomography observations could influence the microstructure of the reinforcement.

An insight into the geometric evolution of the reinforcement at the meso level is detailed measuring in each cross-section the yarns thickness, width and cross-sectional area. These information show the ability of the yarns to deform (i.e. change the shape) and to compact (i.e. change the cross-sectional area) in the considered architecture after shear loading [22]. The cross-sectional shape of the yarns was outlined by six points, as depicted in Fig. 4. To measure the shape parameters of the yarns on micro-CT images, a script was implemented in ImageJ Software [23]. It calculates the coordinates of the points outlining the yarn, matches the coordinates describing a figure, by means a convex envelope algorithm, and, finally, computes the yarns centroid, area ($S$), thickness ($h$) and width ($w$) (see scheme in Fig. 4). The last two parameters are the maximum height and width of the quadrilateral surrounding the convex envelope.

In order to observe the evolution of the yarns shape parameters due to shear deformation, the quantities $S/S_0$, $h/h_0$ and $w/w_0$ were defined as: the ratio of the shape parameter of interest (yarn cross-sectional surface '$S$', width '$w$' or thickness '$h$') in the deformed state, with respect to the same parameter in the undeformed configuration (subscript '0') detailed in Table 2. Furthermore, considering the symmetric distribution of the yarn cross-sections in the fabric unit cell (see Fig. 1), some yarns cross-sections can be considered equivalent (e.g. cross-sections: CS1, CS3 in Fig. 4a; CS1, CS2, CS7, CS8 and CS3, CS4, CS5, CS6 in Fig. 4b). Therefore, average value of $S/S_0$, $h/h_0$ and $w/w_0$ of equivalent yarns cross-sections are detailed. The evolution of the warp and weft yarns cross-section shape parameters for different level of shear deformation, in the 18 positions analyzed (Fig. 5), is illustrated in Figs. 6 and 7.

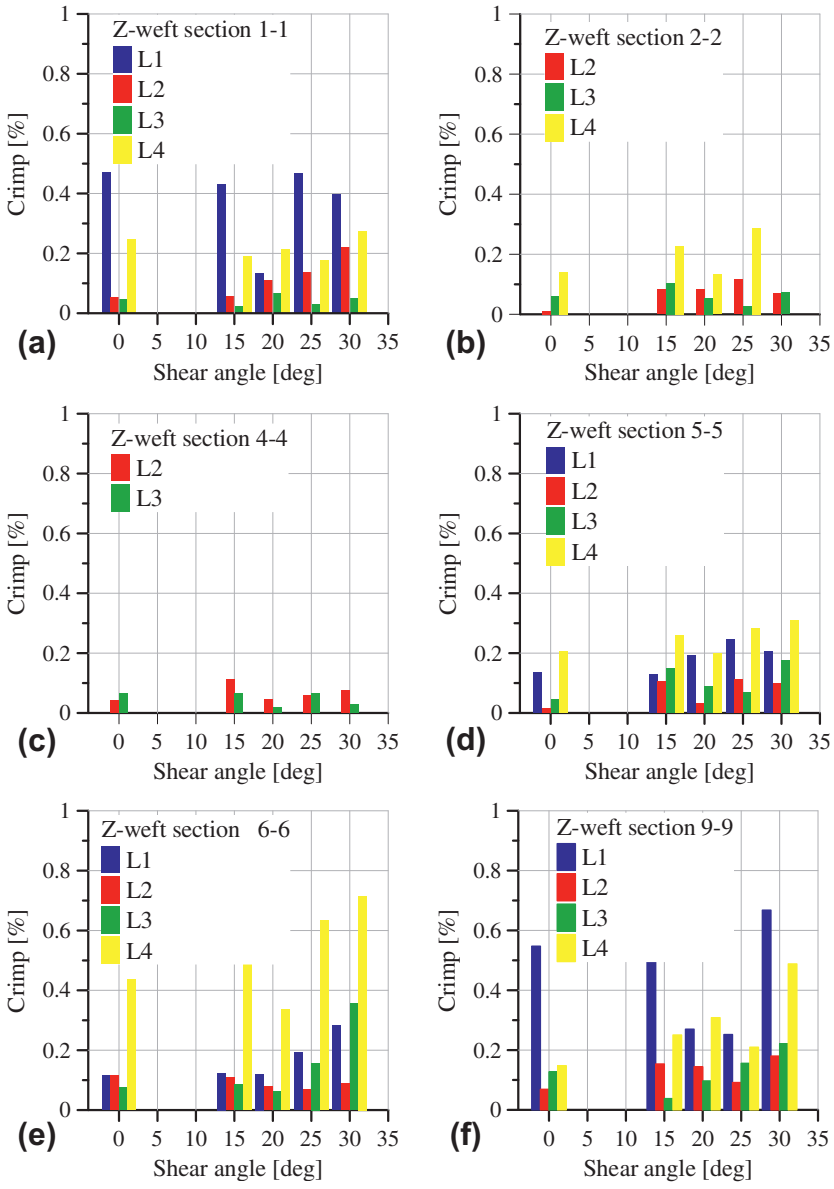


**Fig. 10.** Weft yarns crimp variation vs. shear angle, for positions: (a) 1-1; (b) 2-2; (c) 4-4; (d) 5-5; (e) 6-6; and (f) 9-9 in Fig. 5a.

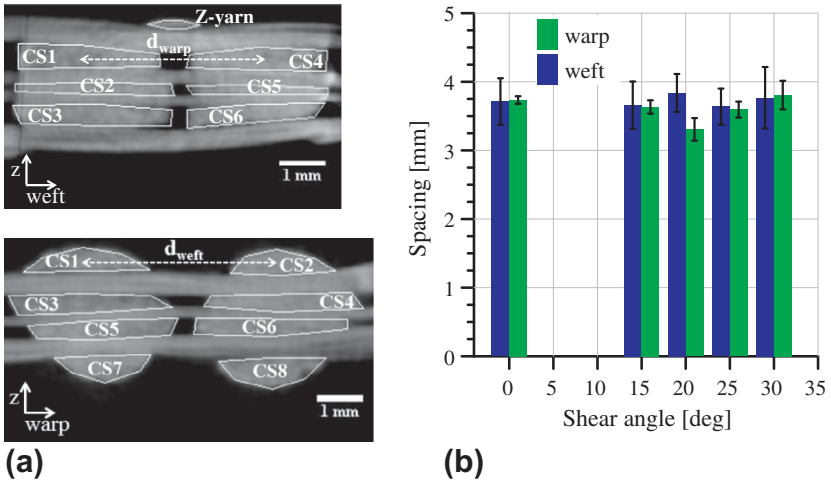


**Fig. 11.** (a) Scheme for measurement of the yarns spacing ($d_{warp}$, $d_{weft}$); (b) warp and weft yarns spacing vs. shear angle. Error bars give the standard deviation.

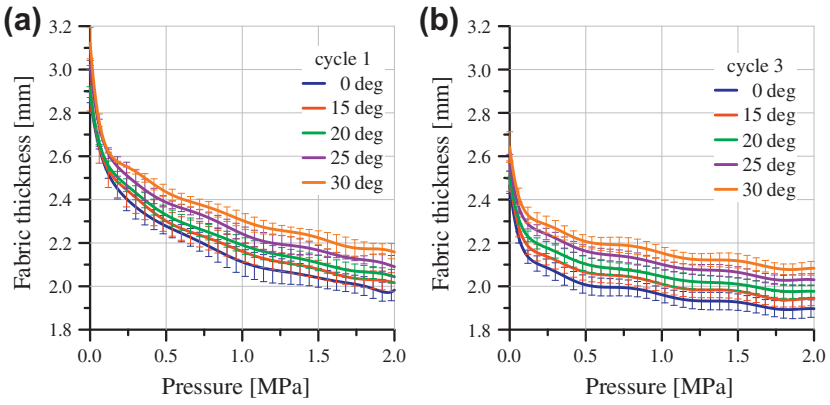


**Fig. 12.** Shear and transversal compression tests. Average fabric thickness vs. compaction pressure curves of specimens sheared at 0°, 15°, 20°, 25°, and 30°; compressive loading (a) cycle 1; (b) cycle 3. Error bars give the standard deviation.

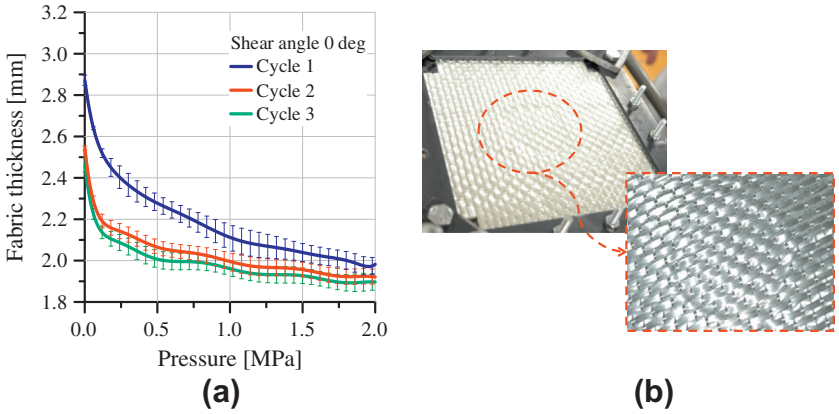


**Fig. 13.** (a) Average fabric thickness vs. compaction pressure curves, for three compression load cycles of un-sheared specimens (error bars give the standard deviation) and (b) permanent deformation after loading.

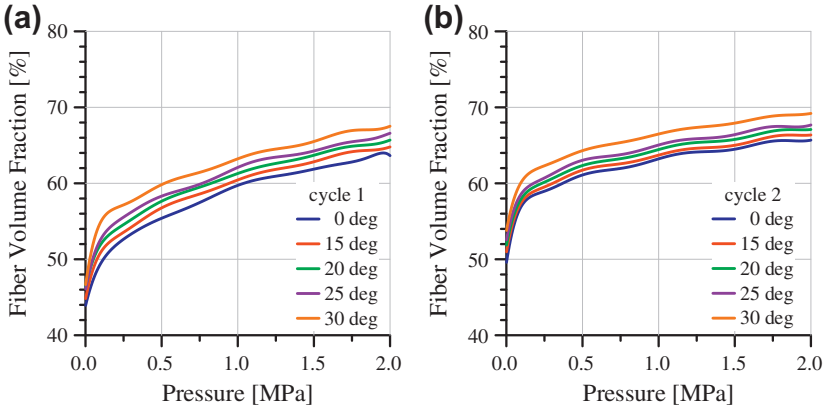


**Fig. 14.** Prediction of fabric fiber volume fraction vs. compaction pressure vs. shear angle (0°, 15°, 20°, 25°, 30°), for (a) the first and (b) the second compression loading.

The shear angle has a slight effect on the warp yarn cross-section width (Fig. 6c and f). Slight reduction (≈5%) is recorded for 20°, while a slight increase is for 30°. On the other hand, the thickness of the warp yarn increase or decrease with respect to the undeformed shape according to the section position, with a relevant increment of ≈40% for the inner one (CS2) (Fig. 6e). The cross-sectional surface of the warp yarn has a similar trend to the thickness.

The width of weft yarns show the same slight variation observed for the warp ones (Fig. 7c and f). The Z-yarns do not allow considerable variation of the width increasing the shear angle. The weft yarn thickness has considerable increment only for a shear deformation of 30° (Fig. 7b and e) with an increase in the range 10–20%. A reflection of this variation is observed on the cross-sectional surface (Fig. 7a and d).

*4.1.2. Warp and weft yarns crimp*

Examples of crimp measurement of the yarns in one cross-section 'Z-warp' and one 'Z-weft' are reported in Fig. 8. The shape of

each longitudinal yarn was outlined by 18 points, as shown in Fig. 8a and c. The crimp of warp and weft yarns was quantified as:

$$crimp = \frac{l_{yarn} - l_{cell}}{l_{cell}} \quad (1)$$

where $l_{yarn}$ is the yarn length calculated as the sum of straight segments between the measurement points in the yarn mid-line; and $l_{cell}$ is the yarn length considered as straight (i.e. distance between end points A and B in Fig. 8b and d). The adopted procedure is similar to the one detailed in [6] with optical microscopy images.

The comparison of the crimp for different shear angles is performed on twelve of the eighteen positions depicted in Fig. 5. Z-yarns do not allow the complete identification of weft and warp longitudinal yarns shape in planes 3-3, 7-7, 8-8 of Fig. 5a; and 1-1, 5-5, 9-9 of Fig. 5b. Moreover, for few Z-weft images (2-2 and 4-4) the top and bottom yarns are not clearly defined and measurements are not reported.

The warp yarns show an increase of crimp with the shear angle (Fig. 9). The most relevant variation of the longitudinal shape is for shear deformation above 25° mainly for the yarns closest the through thickness yarns (positions 4-4, 6-6 and 8-8).

The highest crimp is in the top (L1) and bottom (L4) weft yarns for any shear angle at the Z-yarns cross-overs (positions 1-1, 6-6 and 9-9, Fig. 5a), as expected according to the layup (Fig. 1). Crimp of weft yarns is generally greater than the warp one. The increase of shear angle has a reduced effect on the weft yarns crimp, compared to the warp ones.

The crimp measurements in some cross-sections (Figs. 9 and 10) of the unsheared reinforcement is comparable to the data mentioned in [6] for a carbon/epoxy composite material having a similar 3D textile architecture reinforcement. In [6] the slightly lower values depend on the reinforcement compaction during infusion.

#### 4.1.3. Warp and weft yarns spacing

Yarns spacing was measured for each imposed shear angle, as the average distance between the centroids of adjacent yarn cross-sections (see Fig. 11a), for the 18 positions analyzed (Fig. 5). Hence, for each shear angle, spacing was averaged over a total of: 27 measurements for warp yarns and 36 measurements for weft yarns. Unlike, Z-weft cross-sectional analyses (see Section 4.1.1), for spacing measurements also the edge yarns were considered (see Fig. 11a). Spacing was quantified following the procedure detailed in [5]. The results are depicted in Fig. 11b. The distance between yarns is very similar in the warp and weft directions for the considered shear deformations, except for the shear angle 20° for which the warp yarns have an average distance about 12% lower than the weft counterpart. Moreover, increasing the imposed shear angle the distance of yarns remains approximately unchanged. This is due to the constrain effect of the Z-yarns.

### 4.2. Shear and out-of-plane compression for fabric thickness measurements

The influence of the shear deformation on the thickness variation during molding of the considered 3D reinforcement has been measured by compression tests as detailed in Section 3.3. The fabric thickness as function of the compaction pressure and of the shear angle has been measured with three specimens for each shear angle, namely 0°, 15°, 20°, 25° and 30°. Fig. 12 details the average diagrams of three specimens recorded in three consecutive compression quasi-static loading cycles. The thickness after the first loading cycle shows a permanent reduction (≈10% for 0° and ≈13% for 30° shear angle). This is consequence of the reinforcement compaction that remains permanent as observed in Fig. 13b. This 'plastic' variation of the thickness is completely applied after the first compressive loading (in the range of pressure considered) being the second and the third cycles very close each other (see e.g. Fig. 13a for 0° shear angle). This observation is valid for all the imposed shear angles.

The measured average thickness ($h$) is converted to fabric fiber volume fraction ($V_f$) assuming the fabric areal density ($A$) and the glass fiber density ($\rho$). The fiber volume fraction is estimated by:

$$V_f[\%] = \frac{A}{\rho h \cos(\gamma)} \quad (2)$$

Eq. (2) provides the fabric fiber volume fraction as a function of the applied pressure and the shear angle ($\gamma$), as illustrated in Fig. 14.

Fiber volume fraction ($V_f$) is about 44% and 47% for the unsheared and 30° sheared reinforcement, respectively, at the beginning of the first compression loading, when no transverse pressure is applied. The nonlinear variation of the thickness, increasing the transverse pressure, generates an increase of $V_f$ of about 45% at the maximum applied compression (2 MPa) in the first compression loading. While, the irreversible deformation introduced after the first compression cycle leads to an increase of $V_f$ of about 30% at the maximum pressure level of the second loading cycle. This is valid for all the imposed shear angles (see Fig. 14).

The thickness recorded could be sensitive to the measurement technique. Therefore, to assess the above results, the fabric thickness was measured by X-ray micro tomography (micro-CT) on specimens deformed with different shear angles (see e.g. Fig. 15a). The above mentioned 18 (9 Z-weft and 9 Z-warp) cross-sectional images of one specimen for each shear angle have been adopted to average the thickness in different positions.

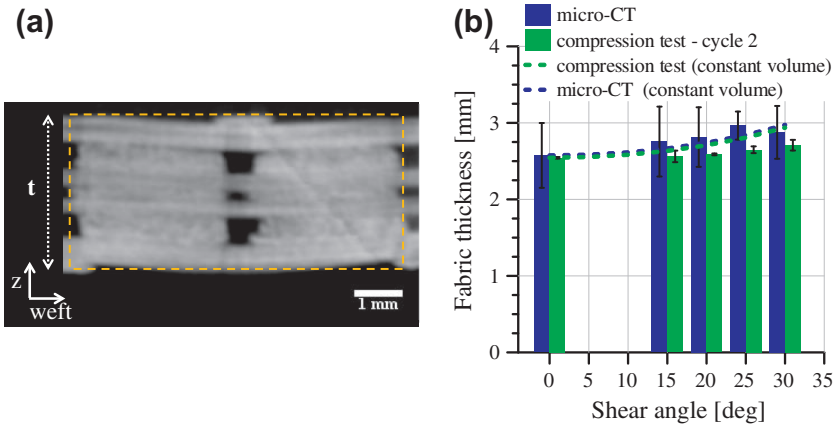


**Fig. 15.** (a) Scheme of fabric thickness ($t$) measurement by micro-CT cross-sectional image. (b) Comparison of thickness measurements by compression test and micro-CT: average thickness vs. shear angle. Error bars give the standard deviation.

Micro-CT and compression tests (at the initial pre-load of 5 N of the second cycle) measurements are compared in Fig. 15b for shear angles of 0°, 15°, 20°, 25° and 30°. The two techniques show values within the scatter band of the measurements. The thickness measured after the second compression loading are, for sheared specimens, underestimated of about maximum 8% with respect to the micro-CT data. The slight difference is explained considering the permanent thickness reduction after the first loading and the initial pre-load adopted in the compression test.

In the industrial practice, the fabric thickness under shear loading is sometimes estimated assuming the invariance of the volume, with all reservations on applicability of this principle to fibrous materials (see e.g. [26]). In Fig. 15b, the measured variation of the thickness with the two techniques is compared to the estimation assuming constant volume. This hypothesis gives satisfactory predictions compared to the micro-CT and compression tests experimental results. It suggests that the thickness variation of this fabric occurs almost at constant volume when a physical constrain compresses transversely the textile (i.e. a punch in compression tests and resin in micro-CT specimens). The same behavior has been observed for carbon fabrics in [26]. Different conclusion is given in [10], where the thickness of the same 3D glass reinforcement was measured by a laser device. The constant volume assumption does not comply with that measurements (the measured thickness increased with shear faster than predicted by the constant volume assumption). The disagreement is probably explained by the fact that the laser method is contactless and applies no transverse constraints on the fabric. In composite production these constraints are always applied, by a mould surface or a vacuum bag. The qualitative discrepancy between the results shows that a contactless technique could be unsuitable in measuring the thickness of a deformed composite reinforcement.

## 5. Conclusions

The investigation presented in the paper analyzes the geometry at the unit cell level of a single layer E-glass non-crimp 3D orthogonal woven reinforcement (commercialized under trademark 3WEAVE® by 3Tex Inc.). The shape of the yarns is observed and measured by X-ray micro-computed tomography (micro-CT) images. One important achievement is the measurement of the internal geometry after different level of imposed sheared deformation, being this considered as the primary deformation mechanism during shaping. Increasing the shear angle, the Z-yarns maintain unchanged the distance between the yarns and as consequence a reduced variation of the yarn cross-section width. The containing effect of the Z-yarns on the thickness of the yarns is mainly visible in the weft direction. A considerable increase of the thickness is observed only after a shear deformation of 30°. The gathered geometric information has a relevant importance in the generation of accurate virtual models for numerical simulations with such 3D composite reinforcement.

Another important achievement is the measurement of coupled effect of shear deformation and transversal pressure on the fabric thickness. The compression tests of sheared specimens reproduce the thickness variation during manufacturing phases like forming and molding of the 3D reinforcement and, as consequence, allow the prediction of the composite material fiber volume fraction.

## Acknowledgements

3Tex Inc. is acknowledged for manufacturing and supplying the non-crimp 3D orthogonal weave E-glass reinforcement (3WEAVE®). The research visit of J. Pazmino to K.U. Leuven was partially supported by INFUCOMP (FP7) project. The help of laboratory staff of the Department MTM – Kris van der Staey – is gratefully acknowledged.

## References

[1] Boisse P. Composite reinforcements for optimum performance. Woodhead Publishing Limited; 2011.
[2] Polturi P, Parlak I, Ramgulam R, Sagar TV. Analysis of tow deformations in textile preforms subjected to forming forces. Compos Sci Technol 2006;66:297–305.
[3] Badel P, Vidal-Sallè E, Maire E, Boisse P. Simulation and tomography analysis of textile composite reinforcement deformation at the mesoscopic scale. Compos Sci Technol 2008;68:2433–40.
[4] Vanaershot A, Cox BN, Lomov SV, Vandepitte D. Stochastic framework for quantifying the geometrical variability of laminated textile composites using micro-computed tomography. Compos: Part A 2013;44:122–31.
[5] Desplentere F, Lomov SV, Woerdeman DL, Verpoest I, Wevers M, Bogdanovich A. Micro-CT characterization of variability in 3D textile architecture. Compos Sci Technol 2005;65:1920–30.
[6] Karahan M, Lomov SV, Bogdanovich, Bogdanovich AE, Mungalov D, Verpoest I. Internal geometry evaluation of non-crimp 3D orthogonal woven carbon fabric composite. Compos: Part A 2010;41:1301–11.
[7] Hivet G, Boisse P. Consistent 3D geometrical model of fabric elementary cell. Application to a meshing preprocessor for 3D finite element analysis. Finite Elem Anal Des 2005;42:25–49.
[8] Nguyen QT, Vidal-Sallé E, Boisse P, Park CH, Saouab A, Bréard J, et al. Mesoscopic scale analyses of textile composite reinforcement compaction. Compos Part B 2013;44:231–41.
[9] Carvelli V, Gramellini G, Lomov SV, Bogdanovich AE, Mungalov DD, Verpoest I. Fatigue behaviour of non-crimp 3D orthogonal weave and multi-layer plain weave E-glass reinforced composites. Compos Sci Technol 2010;70:2068–76.
[10] Carvelli V, Pazmino J, Lomov SV, Verpoest I. Deformability of a non-crimp 3D orthogonal weave E-glass composite reinforcement. Compos Sci Technol 2012;73:9–18.
[11] Ivanov DS, Lomov SV, Bogdanovich AE, Karahan M, Verpoest I. A comparative study of tensile properties of non-crimp 3D orthogonal weave and multilayer plain weave E-glass composites. Part1: materials, methods and principal results. Compos: Part A 2009;40:1134–43.
[12] Mohamed MH, Zhang ZH. Method of forming variable cross-sectional shaped three-dimensional fabrics. US Patent 5085252; 4 February 1992.
[13] Bogdanovich AE, Mohamed MH. Three-dimensional reinforcement for composites. SAMPE J 2009;45:8–28.
[14] Zouari B, Daniel JL, Boisse P. A woven reinforcement forming simulation method. Influence of the shear stiffness. Comput Struct 2006;84:351–63.
[15] Cao J, Akkerman R, Boisse P, Chen J, Cheng HS, de Graaf EF, et al. Characterization of mechanical behavior of woven fabrics: Experimental methods and benchmark results. Compos Part A 2008;39:1037–53.
[16] Chang SH, Sharma SB, Sutcliffe MPF. Microscopic investigation of tow geometry of a dry satin weave fabric during deformation. Compos Sci Technol 2003;63:99–111.
[17] Baruchel J, Buffiere JY, Maire E, Merle P, Peix G. X-ray tomography in material science. Paris: Hèrmes; 2000.
[18] Stock SR. X-ray microtomography of materials. Int Mater Rev 1999;44(4):141–64.
[19] Schilling PJ, Karedla BPR, Tatiparthi AK, Verges MA, Herrington PD. X-ray computed microtomography of internal damage in fiber reinforced polymer matrix composites. Compos Sci Technol 2005;65:2071–8.
[20] Lambert J, Chambers AR, Sinclair I, Spearing SM. 3D damage characterisation and the role of voids in the fatigue of wind turbine blade materials. Compos Sci Technol 2012;72:337–43.
[21] Pandita SD, Verpoest I. Prediction of the tensile stiffness of weft knitted fabric composites based on X-ray tomography images. Compos Sci Technol 2003;63:311–25.
[22] Badel P, Maire E. X-ray tomography analysis of the mechanical behaviour of reinforcements in composites. In: Composite reinforcements for optimum performance. Woodhead Publishing; 2011. p. 565–87.
[23] Rasband WS. ImageJ, US National Institutes of Health, Bethesda, Maryland, USA; 1997–2005 <http://rsb.info.nih.gov/ij/>.
[24] Kerckhofs G, Schrooten J, Van Cleynenbreugel T, Lomov SV, Wevers M. Validation of X-ray microfocus computed tomography as an imaging tool for porous structures. Rev Sci Instrum 2008;79(1):1–9. No. 013711.
[25] Van Bael S, Kerckhofs G, Moesen M, Pyka G, Schrooten J, Kruth JP. Micro-CT-based improvement of geometrical and mechanical controllability of selective laser melted $Ti_6Al_4V$ porous structures. Mater Sci Eng A 2011;528:7423–31.
[26] Lomov S, Barburski M, Stoilova T, Verpoest I, Akkerman R, Loendersloot R, et al. Carbon composites based on multiaxial multiply stitched preforms. Part 3: biaxial tension, picture frame and compression tests of the preforms. Compos: Part A 2005;36:1188–206.